Advances Toward a Lightweight, Variable Fidelity Wake Simulation Tool

Joseph Saverin, D Marten, N Nayeri and CO Paschereit

Chair of Fluid Dynamics, Technical University of Berlin, Berlin, Germany

E-mail: `j.saverin@tu-berlin.de`

Abstract. A method is presented which aims to bridge the gap between overly simplified momentum-based wake models and overly demanding finite volume models of wind turbine wake evolution. The method has been developed to allow an essentially user-defined resolution of the wake. Beyond this, all dominant field quantities are automatically resolved by the solver including convection velocity, shear stress and turbulence intensity. Two distinct methods of solution are presented which both have strengths and weaknesses, the choice of which model being fidelity and application dependent. Both methods make use of multilevel spatial integration to allow greatly improved computational efficiency. The method is here presented for 2D flow in the symmetry plane of a vertical axis wind turbine as an initial demonstration of the potential of the method.

1. Introduction and Physical modelling

The progression of the wind turbine industry towards higher order aerodynamic models in the aerodynamic design of wind turbines is necessitated by the greater challenges facing modern wind turbine designers including but not limited to: turbulent inflow, offshore turbines and aeroelastics, the latter becoming increasingly prominent due to the general trend toward larger turbine blades. Accurate modelling of unsteady loads due to the aforementioned factors make the possibility of discarding lower order momentum-based methods in favour of higher order vortex particle or filament methods increasingly attractive. A significant amount of research has already been devoted to examining these models and the effects that they have on predicting fatigue loading and performance of a wind turbine [1, 2]. For reasons of adaptability and amenability to optimised and parallel programming, the work here adopts vorticity-based methods, which allow a Lagrangian treatment of the flow field [3]. Furthermore, by specifying characteristic simulation grid size, the user is essentially capable of tailoring the simulation fidelity for desired modelling outcomes. These methods are also amenable to acceleration by their inherent formulation by separating near and far-field influence. The general method of solution is to make use of the fast-multipole method [4] to treat the far-field interactions. The work here however makes use of the recently introduced multilevel integration method [5]. The application of this method to such high order modelling has, to the author's knowledge, not yet been significantly explored. The application of vortex particle (VP) methods has been chosen here as it allows for all important wake features to be inherently treated [6]. This includes unsteady aerodynamics, trailing and bound vortex shedding, wake velocity self-induction, vorticity strength evolution, vortex merging and destruction and modelling of turbulent effects [7]. The ability of such

models to accurately predict higher order unsteady aerodynamics without incurring exorbitant computation expense brings the treatment of inherently more difficult flow problems, such as multiple turbine interaction, wake breakdown and wake augmentation, closer towards the design environment and allows for improved and optimised turbine and farm design.

1.1. Equations and the Vortex Particle Method

The evolution of vorticity for an incompressible, Newtonian fluid must obey the following equations:

$$\nabla \cdot \vec{u} = 0 \; , \qquad \frac{d\vec{\omega}}{dt} = \frac{\partial \vec{\omega}}{\partial t} + (\vec{u} \cdot \nabla)\vec{\omega} = (\vec{\omega} \cdot \nabla)\vec{u} + \nu\,\nabla^2\vec{\omega} \qquad (1)$$

These pertain to conservation of mass (continuity equation) and conservation of momentum (vorticity transport equation), respectively. Recalling that vortex filaments behave as material lines for an inviscid flow [8], the field can be represented as a particle set and tracked in a Lagrangian sense. The vorticity field is then represented as the sum of a set of vortex particle p, each with position $\vec{x}_p$, vorticity $\vec{\omega}$ and characteristic volume ΔV_p:

$$\vec{\omega}_\sigma(\vec{x}) = \sum_p \vec{\omega}_p\,\Delta V_p\,\zeta(\rho) \qquad (2)$$

where $\zeta(\rho) = \zeta((\vec{x} - \vec{x}_p)/\sigma_p)$ is a regularisation function, introduced to remove singular behaviour from the field. This form of solution is referred to as the vortex particle (VP) method. The velocity field $\vec{u}(\vec{x})$ is computer from the vorticity field via the stream function $\vec{\psi}$ which satisfies the relation $\nabla^2\vec{\psi} = -\vec{\omega}$. The Green's function for $-\nabla^2$ in an unbounded domain is given by: $G(\vec{x}) = 1/(4\pi|\vec{x}|)$, which allows for convolution over the particle field: $\vec{\psi} = G(\vec{x}) * \vec{\omega}(\vec{x})$ where $*$ is a convolution operator. For more details the reader is referred to Winckelmans [9]. There now two methods which allow for the calculation of the velocity field $\vec{u}$, both of which are based upon the solution of the Poisson equation for the stream function: $\vec{u} = \nabla \times \vec{\psi}$.

Method 1: Greens Function   The velocity can be extracted by convoluting equation 1.1 above:

$$\vec{u} = \nabla \times \vec{\psi} = \sum_p \vec{K}_u(\rho) \times \omega_p\,\Delta V \qquad (3)$$

where $\vec{K}_u(\rho)$ is the well-known Biot-Savart kernel for a regularized vortex particle. Analytical expressions are known for this kernel based on the regularisation ζ chosen [9]. The evaluation of the velocity at a field points $\vec{x}$ hence amounts to a sum over the influence of each particle. This shall be further detailed in the following section.

Method 2: Poisson Solver   If the spatial distribution of $\vec{\psi}$ is known, then the velocity can be directly extracted by calculating $\frac{\partial \psi_i}{\partial x_j}$ using finite differences. The solution to the Poisson equation over a spatial domain $\mathcal{P}$ has been the focus of significant research and highly optimised commercial solvers are available which make use of either spectral methods [10] or multigrid methods [11]. In order to attain the solution, boundary conditions (**BC**) for ψ must be specified over the boundary of $\mathcal{P}$. The most generally applicable approach to this is to specify Dirichlet BC's for $\vec{\psi}$ on the domain of interest. This has the added advantage that $\mathcal{P}$ can be specified to compactly enclose the vortical region of interest. This is a significant advantage this method has over finite volume (FV) solvers, as only the domain of interest is required in the calculation. This method has been successfully applied before to general 3D VP solvers [7].

Analog to the expressions for $\vec{K}_{\sigma,u}$ above, there exists analytical expressions for the stream function Kernel $\vec{K}_{\sigma,\psi}$. Fast Poisson solvers require a uniform spatial grid, and hence the disordered particle distribution must be appropriately mapped to an underlying uniform grid [12].

1.2. Spatial Integration- Multilevel Method

Regardless of the method of solution, the particle set must be spatially integrated in order to determine the influence at each field point. This incurs a non-negligible computational expense which constitutes the bulk of the task. This computational expense can be massively reduced by making use of the multilevel method, which makes use of a hierarchical spatial coarsening to approximate particle influence in the far-field [5]. The calculation can be broken into two segments:

Far-Field Evaluation   The particle strength distribution is adjoint interpolated (anterpolated) onto a regular spatial grid. This is then further further anterpolated onto progressively coarser spatial grids- as illustrated diagrammatically in Figure 1. The interaction between boxes is calculated under the assumption that at these distances the influence can be approximated by a singular source particle (ignoring regularization). This shall be demonstrated for the kernels of interesting in the proceeding section. The symmetry between each box-family allows the interaction for a given volume to be pre-calculated and expressed as a simple matrix multiplication saving significant overhead. The accuracy of the anterpolation-interpolation is controlled by the order of the interpolation P. This factor dictates the number of points in each spatial direction onto which the anterpolation/interpolation occurs. For the case illustrated in Figure 1, $P = 2$.
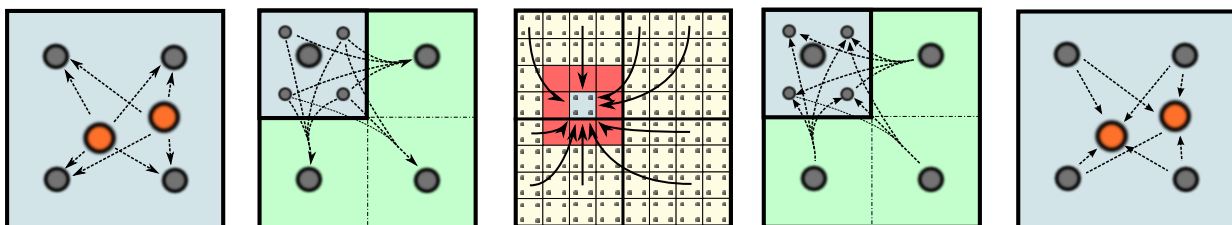

Figure 1. The method of solution of the multilevel method. From left to right: Base anterpolation: Source particle strengths are transferred to grid nodes. Anterpolation: Grid strengths are progressively transferred to courser grids. Interaction: Interaction between grid boxes is carried out. Interpolation: Influence is interpolated to finer grids. Base interpolation: Influence of far-field interpolated onto source nodes / probe nodes.

Near-Field Evaluation   In the near-field, where the polynomial approximation of the source is inaccurate the receiver-source interaction is calculated directly. The size of the region around which the near field is directly calculated is dictated by the factor H, which represents the minimum box size. For source particles within neighboring boxes, the interaction is calculated directly using the Green's functions.

The method has successfully been applied to the 3D Biot-Savart Kernel $K_{u,3D}$ [13, 14, 15]. In the aforementioned works the 3D Biot-Savart Kernel was accurately captured for the determination of the convection velocity and the application of the method to higher order

effects in 3D flows is currently under way. The work here is a step towards demonstrating the ability of the code to capture higher order effects, including viscous effects and turbulence for 2D flow, and is now described for the two modelling approaches. It shall be assumed from this point on, that a Gaussian type smoothing is used.

Method 1: Greens Function: Multilevel far-field   In this case the multilevel method is used to approximate the Biot-Savart Kernel in 2D for the convection velocity. This is given by:

$$K_{u,2D} = \frac{1}{2\pi} \left[\left(\frac{x - x_p}{r^2} \right) \vec{e}_x + \left(\frac{y - y_p}{r^2} \right) \vec{e}_y \right] (1 - e^{-\frac{\rho^2}{2}}) \tag{4}$$

One immediately observes that the function $g(\rho) = 1 - e^{-\frac{\rho^2}{2}}$ asymptotes very quickly to unity, and the approximation $g = 1$ for $\rho > 5$ is generally acceptable. The solver for this method shall hereafter be referred to as the Vortex Particle Multilevel (VP-ML) method.

Method 2: Poisson Solver: Multilevel far-field   The expression for the stream function induced by a 2D vortex particle is given by:

$$\psi_{u,2D} = \frac{1}{4\pi} \left\{ \log \left(\frac{\rho^2}{2} \right) + E_1 \left(\frac{\rho^2}{2} \right) \right\} \tag{5}$$

where E_1 is the exponential integral. The exponential integral decays very quickly and for $\rho > 5$ its contribution can be taken as negligible. The remaining term $\log(\frac{\rho^2}{2})$ presents difficulties in the far-field due to the scaling with respect to the characteristic coresize σ. By expanding out the expression, one has for the stream function in the far-field the following: $\psi_{ff} = log(r^2) - log(\sigma^2) - log(2)$. This can be pre-calculated for a box-receiver template as outlined earlier, however must be scaled appropriately for each higher grid level. The leading far-field term for grid level n becomes: $\log(2^n r^2) = n \log(2) + 2 \log(r)$. The practicality of the multilevel method can hence be fully exploited. The solver for this method shall hereafter be referred to as the Vortex Particle- Mesh Multilevel (VPM-ML) method.

1.3. Field Quantities
The resolution of the necessary quantities shall be described.

1.4. Viscous Effects
The resolution of the Laplacian of vorticity $\nabla^2 \vec{\omega}$ is necessary to ensure viscous effects in the flow are captured. These are crucial for the modelling of vortex merging or destruction, important physical processes in wake breakdown.

VP-ML Method   The method of particle strength exchange (PSE) approximates the Laplacian with an integral operator. The method has been shown to accurately capture viscous effects provided that particle overlap is maintained [16, 9].

VPM-ML Method   The Laplacian is approximated on the grid by making use of an isotropic finite difference stencil as described in Cocle [7].

Turbulent shear stress   In the approach taken here, a large eddy simulation (LES) approach is taken. Here the most energetic scales are resolved and the effect of sub-grid scales (SGS) is modelled. For the purpose of it's simple implementation, a simple hyper viscosity model is used.

$$\frac{d\omega_T}{dt} = -\frac{C}{T_0}(h^2\nabla^2)^2\omega \tag{6}$$

where C is a coefficient and T_0 a global time scale. This makes use of the Laplacian scheme as implemented above to calculate an additional rate of change of vorticity term. Although not displayed here, the model also automatically captures the shear stress terms of the strain rate tensor S_{ij}, which implies that the model could also be used for higher order turbulence modelling, such as that detailed in Jeanmart et al. [17] or Cocle et al. [7].

2. Validation

The validation of the solver shall proceed as follows. First validation that the multilevel method functions for the calculation of the i) Biot-Savart kernel for the VP-ML method, and ii) the stream function kernel for the VPM-ML method is demonstrated. Following this the capturing of important physical quantities is described including convection, viscous velocities and turbulence parameters.

2.1. Multilevel far-field behaviour

For both bases the relative E_{L2} type error is given, where $E_{L2} = L_2(\Delta\vec{x})/L_2(\vec{x})$ error is shown, where $L_2(\vec{a}) = \frac{1}{n}\sum_n(|\vec{a}|)^2$. The influence is carried out on a particle set corresponding to the wake behind a vertical axis wind turbine (VAWT), as demonstrated in the application section. The value of the calculated influence at each vortex particle position $\vec{I}(\vec{x}_p)$ is compared to the value calculated directly from the Green's function method $\vec{I}_D(\vec{x}_p)$, from this the error metric is calculated $L_2(\vec{I}(\vec{x}_p) - \vec{I}_D(\vec{x}_p))$.

Multilevel Treatment of Biot-Savart Kernel   This kernel is applied when using the VP-ML method. As seen in Figure 2, the behaviour of the multilevel method is well predicted and generally it can be seen that the error due to the multilevel far-field approximation is seen to generally decrease with increasing minimum box-size H, this is intuitive as the larger H, the larger region is directly calculated. It can also be observed that the error plateaus beyond a certain polynomial approximation order P, this is the point at which the error incurred by the far-field approximation cannot be recovered. The choice of H and P is then hence a matter of desired accuracy. It can also be observed that, provided H has been adequately chosen, P scales logarithmically, and therefore each increase in P reduces the error by a factor of 10.

Multilevel Treatment of Stream Function Kernel   This kernel is applied when using the VPM-ML method. Figure 2 shows the error as a function of polynomial order. Similar behaviour is observed for the stream function kernel as was seen for the Biot-Savart kernel. An initially linear behaviour, followed by a plateau. This is fundamentally of interest, as the logarithmic function in the stream function kernel is monotone increasing, as opposed to monotone decreasing for the $1/r^2$ factor in the Biot-Savart kernel. This implies that the total contribution to the stream function from far-field points may contribute more to the total influence. The behavior of the velocity field however is in fact dependent on the gradients of the stream function $\nabla\psi_z$. The stream function in the 3D case has again a far-field behaviour similar to the Biot-Savart kernel.
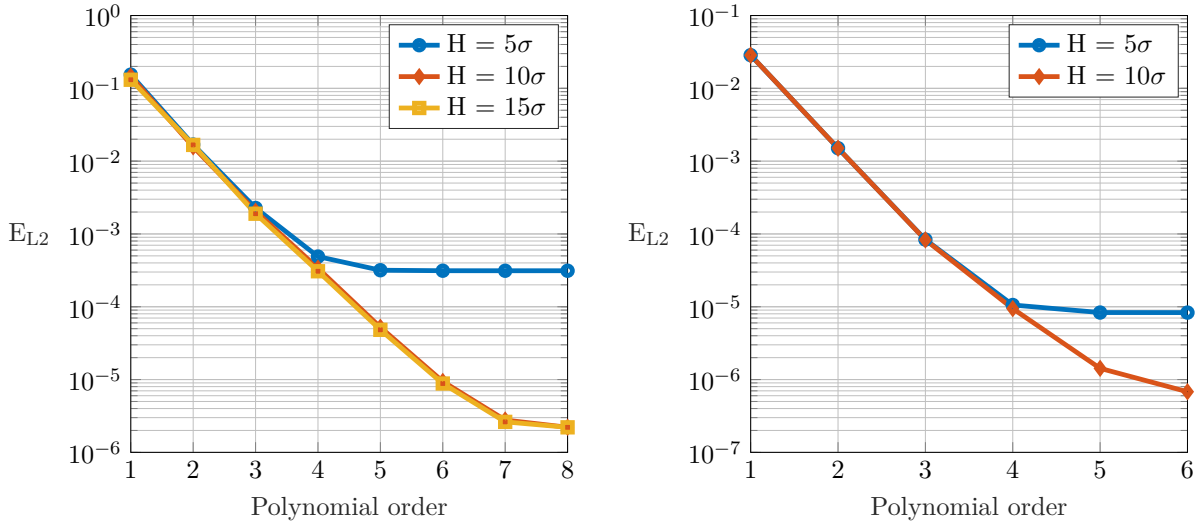
Figure 2. Relative error E_{L2} as a function of polynomial order P for the 2D Biot-Savart kernel (left) and the 2D stream function kernel (right).

2.2. Convection Velocities

In order to validate that the calculation of the convection velocities, an inviscid test case has been chosen which furthermore is aimed at capturing important dynamics of vortex set evolution. This is the case of an initially elliptical vortex distribution, as detailed in Koumoutsakos [18], where the equivalent VP simulation has been carried out however with the use of a multipole method. It should be noted that in that work the results were also compared to experiments in pure electron plasmas of Driscoll & Fine [19], which can be shown to mimic the field equations of an inviscid fluid. The particle set parameters such as coresize σ, grid size H (overlap) are as defined in the comparison paper. A Gaussian regularisation $\zeta(\rho)$ has been used. To ensure particle overlap the particle set is remeshed every five timesteps with the M_4' scheme [12]. The polynomial order $P = 4$ and minimum grid size for the multilevel solver was set to $H = 10\,\sigma$. The particle motion has been integrated with a second-order leapfrog scheme with a timestep of $\Delta t = 2.5 \cdot 10^{-4}s$.

Figure 3 illustrates a number of important flow features. The first is the filamentation of the vortex captured by the solver. The second is the slow axysymmetrisation of the elliptical distribution over time. The resolution of these processes along with a qualitative comparison to the essentially identical evolution in [18] demonstrates accuracy of both solvers. A quantitative comparison is carried out in Figure 4. Here one can see the filamentation process and core narrowing of the vortex.

2.3. Laplacian: Viscous Quantities

Here comparison is made to the viscous case described in Buntine & Pullin [20] of two equally signed Gaussian vortices merging into a stable Burgers vortex configuration. The grid parameters have been chosen as follows: $\sigma = 0.085\,m$, $H = 10\,\sigma$, $P = 4$. As with the inviscid case, remeshing also occurs every five timesteps. For this method the leapfrog method was used to evolve the particle position and a second-order Adams-Bashforth method was used to evolve particle vorticity ω_z, identical to the scheme used in Cocle et al. [7].

The evolution of the vortex set is visualised in Figure 5. The merging of the vortices is clearly captured and the progression towards a stable vortex, precisely as shown in Buntine & Pullin [20] is displayed. Vorticity contours are again identical to those in the given reference, implying
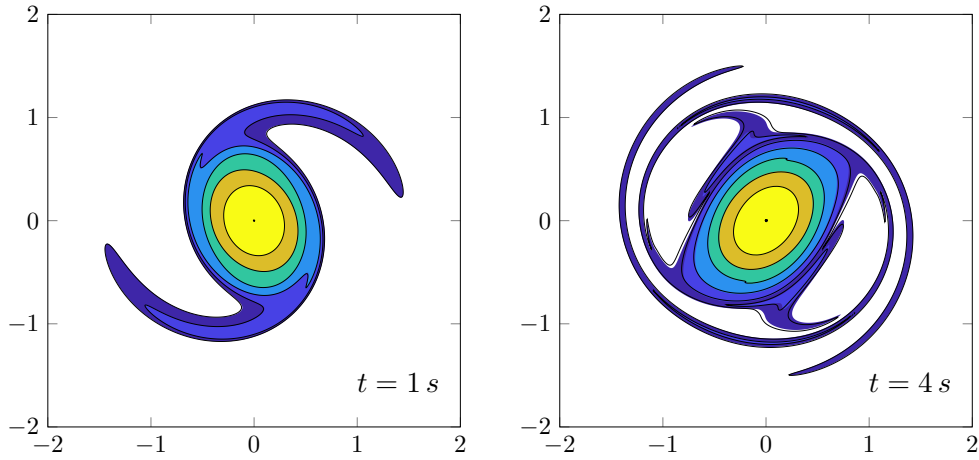
Figure 3. Evolution of the vorticity field of an initially elliptical vorticity distribution. The time evolution of the ellipse is demonstrated for both solvers here. The colour contour plots correspond to the VP-ML solver, contours correspond to the VPM-ML solver. Agreement is seen to be excellent. Contours correspond to $|\omega_z| = 0.25, 2:4:20$.
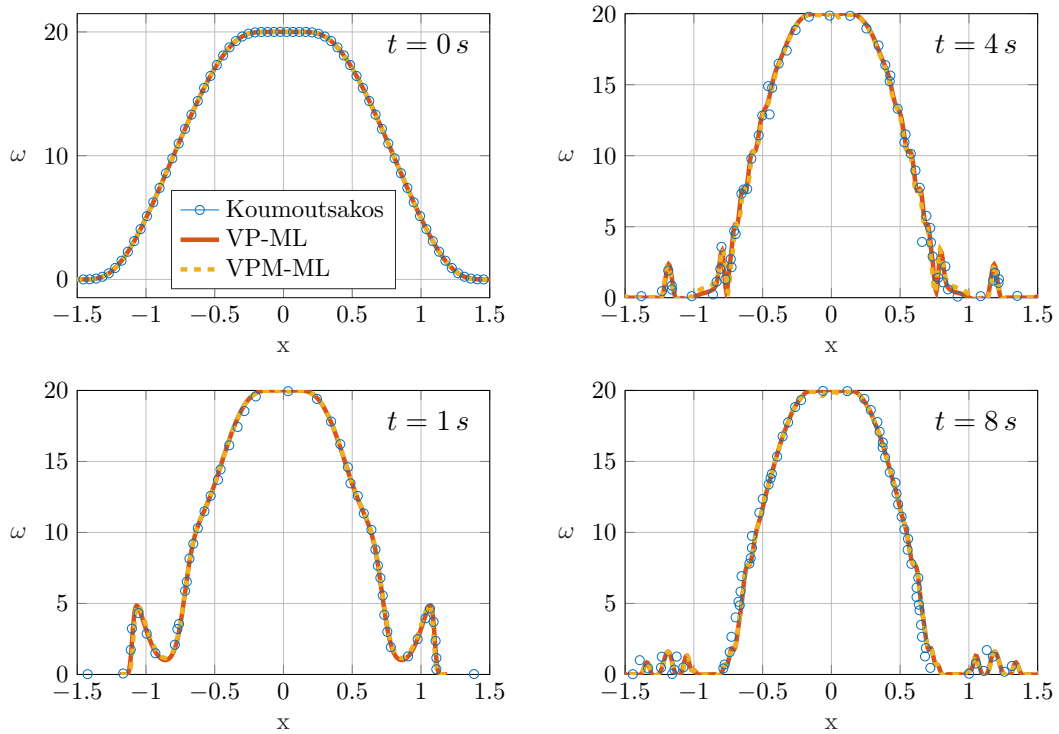

Figure 4. Distribution of ω along the x axis. Comparison to the data of Koumoutsakos [18] shows excellent quantitative agreement in terms of both contraction of the central region of vorticity and filamentation at the vortex perimeter.

a qualitative agreement in the evolution of the simulation. A quantitative comparison is shown in Figure 6 where the results are shown along the axes $x = 0$ and $y = 0$ for a range of time values. The vorticity is seen to agree excellently for a range of time values and the progression
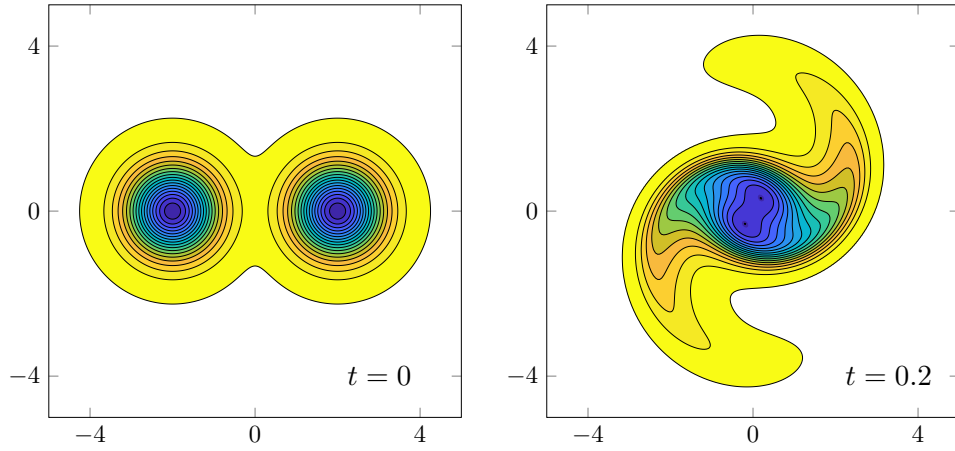
Figure 5. The merging of two initially Guassian vortex distributions. The vortex asymptotes to a stable Burgers' vortex after approximately $t = 0.6\,s$.

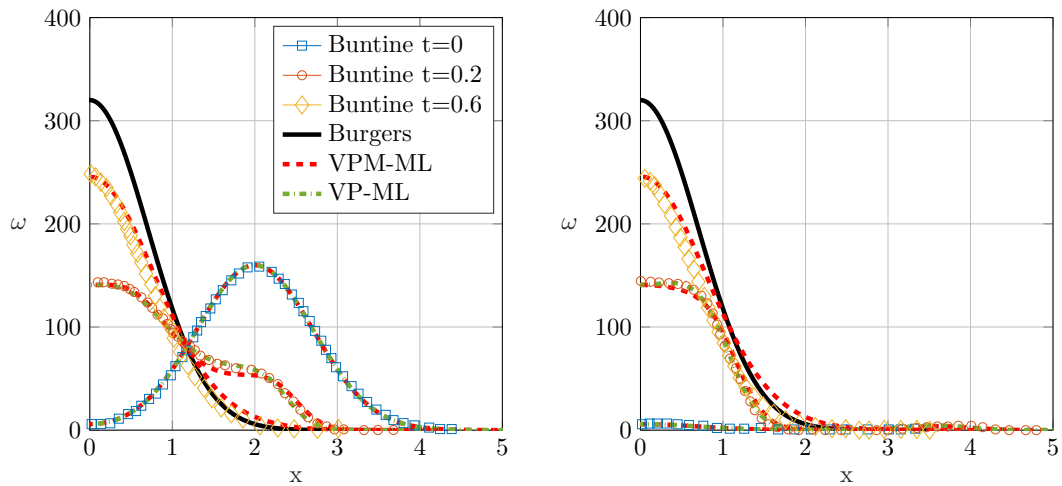of the solution towards that of a stable Burgers vortex is observed.

Figure 6. Evolution of vorticity along the axes $y = 0$ (left) and $x = 0$ (right).

2.4. Hyperviscosity operator

As the hyperviscosity operator (at least for the simplifed SGS approach taken here) is simply calculated by a further calculation using the Laplacian operator, the validation only really requires showing that the Laplacian operator function, this was carried out in the previous section.

3. Application

As the purpose of the work here is an preliminary application of the method to a 2D flow prior to application to a fully 3D flow, a suitable test case must be found. A fitting application is the symmetry plane of the wake of a VAWT as this displays a quasi-2D flow and contains a number of the important flow features which would also occur in the wake of a standard horizontal axis wind turbine.

Generation of vorticity

A simple lifting vortex assumption is made which places the lifting vortex at the quarter chord point of the airfoil. The lift coefficient C_l is extracted from a polar generated with XFoil [21] for the corresponding Reynolds number Re corresponding to the maximum relative velocity U_{rel} seen by the airfoil in undisturbed inflow. The lift from this C_l value is compared to that from the Kutta-Joukowksi theorem and the circulation of the airfoil Γ can be derived. No unsteady effects are considered through for example an unsteady lift model such as the Beddoes-Leishman model [22], as this lies outside of the scope of this work. Kelvin's theorem is then applied to ensure that the change in airfoil vorticity is shed into the wake, this is done at the trailing edge of the airfoil. For the turbine here a NACA0012 profile has been chosen.

Turbine parameters

A three-bladed ($B = 3$) turbine has been taken with a radius $R = 1\,m$, chord length $c = 0.1\,m$. The freestream inflow U_∞ was set to $1\,ms^{-1}$ in positive x direction. Rotational speed Ω of the turbine is set based on the tip speed ratio $\lambda = R\Omega/|U_\infty|$, here set to $\lambda = 6$.

Simulation parameters

A fully viscous simulation with viscous interaction and turbulence generation has been simulated with the VPM-ML method. Although the equivalent is technically possible for the VP-ML solver, the necessity to resolve the viscous terms implies that the solver requires the generation of a number of *dummy* nodes around regions of interest, this has been left for future work. The kinematic viscosity ν was set to that of room temperature air. The grid spacing was set to $H_{grid} = 0.02\,m$. This allows specification of the particle characteristic coresize σ as detailed in Cocle et al. [7]. The multilevel parameters were taken as $H = 10\,\sigma$, $P = 4$. The specification of the grid spacing H_{grid} is the single parameter which requires specification here. Choosing this parameter largely automatically specifies all other important vorticity field parameters, as such the fidelity of the simulation is a user input. A choice of increasingly fine H_{grid} leads eventually to a fully resolved simulation of the wake.

Discussion

Observation of Figure 7 shows that deceleration caused by the blade is clearly captured by the model. Shear layers in the wake are also captured with a region of underspeed behind the rotor and slight overspeed around the rotor. Wake recovery is seen to be occuring at a distance approximately $2D$ downstream of the rotor, however this should only qualitatively be assessed as the thrust and lift coefficients were not accurately validated against an experimental turbine. Visualisation acts only to serve a qualitative purpose. The hyperviscosity operator, necessary for the calculation of the turbulent effects on the evolution of particle strength is visualised also in Figure 7. It is seen that the regions of greatest turbulent action are indeed in the ridges where from inspection of the velocity profile the velocity gradients are strongest. It should be noted that it is expected that the inclusion of this turbulent strength fluctuation should provide the necessary mechanism to correctly capture true wake breakdown in modelling.

4. Conclusion

The treatment of the far-field interaction of a vortex particle method has been demonstrated for a set of 2D flow cases. Important effects such as convection velocity, viscous effects and turbulent modelling parameters are captured. The preliminary application to a 2D application of the wake behind a VAWT is shown to capture important flow quantities in the wake evolution. These results were achieved with the specification of a single field parameter, the grid size H_{grid}, this implies that the fidelity of the simulation is completely user-specified. The task of validation for a 3D flow remains and is currently underway.
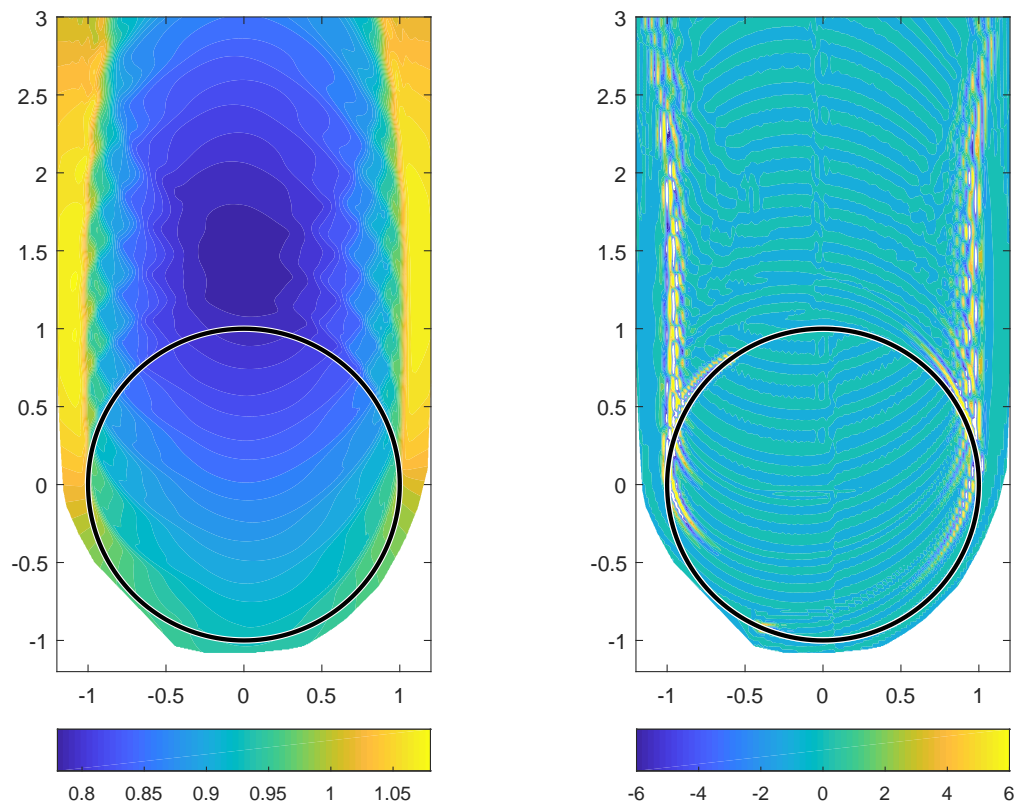
Figure 7. Flow in the wake of an idealized three-bladed VAWT operating at tip speed ratio $\lambda = 3$. Left: Velocity in x direction. This is extracted directly from application of the Biot-Savart kernel on the instantaneous vorticity field. Right: Normalized vorticity hyperviscosity operator $(h^2 \nabla^2)^2 \omega_z$. This parameter is necessary for inclusion of turbulent shear stress terms using the SGS model.

References

[1] Perez-Becker S, Papi F, Saverin J, Marten D, Bianchini A and Paschereit C O 2020 *Wind Energ. Sci. Discuss.* In review URL `https://doi.org/10.5194/wes-2019-70`
[2] Boormsa K, Hartvelt M and Orsi L 2016 *J. Phys. Conf. Ser.* **753**
[3] Branlard E 2017 *Wind Turbine Aerodynamics and Vorticity-Based Methods* (Springer International Publishing)
[4] Greengard L, Carrier J and Rokhlin V 1988 *SIAM J. Sci. and Stat. Comput.* 669–86
[5] van Garrel A 2017 *Proc. AIAA SciTech Forum* (Grapevine, Texas, USA)
[6] Winckelmans G 1989 *Topics in Vortex methods for the Computation of two- and three-dimensional incompressible unsteady flows* Ph.D. thesis California Institute of Technology
[7] Cocle R, Winckelmans G and Daeninck G 2008 *J. Comp. Phy.* 9091–120
[8] Batchelor G 1967 *An Introduction to Fluid Mechanics* (Cambridge University Press)
[9] Winckelmans G and Leonard A 1993 *J. Comp. Phys* **109** 247–73
[10] Canuto C, Hussaini M, Quarteroni A and Zang T 2006 *Spectral Methods: Fundamentals in Single Domains* (Springer)
[11] Briggs W, Henson V and McCormick S 2000 *A Multigrid Tutorial* (Society for Industrial and Applied Mathematics)
[12] Cottet G and Koumoutsakos P 2000 *Vortex Methods: Theory and Practice* (Cambridge University Press)
[13] Saverin J, Marten D, Pechlivanoglou G, Nayeri C and Paschereit C 2018 *Proc. AIAA SciTech Forum*

      (Kissimee, Florida, USA)

[14] Saverin J, van Garrel A, Pechlivanoglou G, Nayeri C and Paschereit C 2018 *ASME Turbo Expo 2018*

[15] Saverin J, Persico G, Marten D, Holst D, Pechlivanoglou G, Paschereit C and Dossena V 2018 *J. Eng. Gas Turbines Power*

[16] Degond S and Mas-Gallic P 1989 *Math. Comp.* **53** 485–507

[17] Jeanmart H W G 2007 *Phys. Fl.* **5** 055110

[18] Koumoutsakos P 1997 *J. Comp. Phys.* 821–857 cP975749

[19] Driscoll C and Fine K 1990 *Phys. Fl.* **6**

[20] Buntine JD P D 1989 *J. Fl. Mech.* 263–95

[21] Drela M and Youngren H 1989 *Conf. Notre Dame* (Notre Dame, Ind (USA))

[22] Leishman J G and Beddoes T S 1989 *Journal of the American Helicopter Society* **34** 3–17